Journal of Engineering Mathematics (2005) 53: 253–269
DOI 10.1007/s10665-005-9015-0

Microwave propagation over the Earth: image inversion

NEV FOWKES and BRETT NENER
Department of Mathematics, The University of Western Australia, 35 Stirling Highway, Crawley, WA 6009, Australia (fowkes@maths.uwa.edu.au, brett@ee.uwa.edu.au)

Received 14 October 2004; accepted in revised form 23 August 2005

Abstract. An extremely accurate but simple asymptotic description for the path of a light ray propagating over a curved Earth with steady radial variations in refractive index is derived using simple scaling arguments. It is used to determine effectively exact analytic solutions for the path of rays through refractive-index profiles described in terms of patched quadratics. Such patched quadratics can be used to accurately describe almost all refractive-index profiles of practical interest. The results show that images generated by rays passing through a quadratic refractive-index profile are uniformly magnified in the vertical direction, and magnification and displacement observations can be used to determine the refractive-index profile parameters. For patched quadratics, observations of critical rays can be used to determine the thicknesses of the quadratic layers.

An effectively exact solution is also obtained for exponential index profiles and this is used to determine the path of rays through a thin boundary layer attached to the Earth; an inferior mirage situation.

Key words: asymptotics, inverse problems, microwave propagation, mirages

1. Introduction

A ship is seen on the horizon; where is it *exactly* and what is its shape? It is not a silly question. Its size and location is not as seen by the eye and interpreted by the brain; for example the location can be misjudged by 10–20 m. The point is that what is seen is determined by the ray paths from the ship to the eye, and light rays do not travel in straight lines. Other more spectacular consequences of the bending of light rays are mirages, and looming. Although not explicitly expressed in the question, the real challenge is to determine the refractive-index profile; we are really dealing with an inverse problem, and this particular inverse problem is known to be very difficult to solve numerically.

Many of the above observations have been qualitatively understood for hundreds of years and quantification came with Willebrord Snell's celebrated law back in 1621. In more recent times geometric optics and variational principles have been used to obtain an implicit path description of a ray propagating through a variable-refractive-index medium; Courant and Hilbert devote a whole chapter to the eikonal equation describing propagating rays. Still more recently multi-scaling ideas have been used to determine accurate asymptotic-solution descriptions close to caustics and to separate out diffraction effects. In spite of all the above, the practical determination of the above ship's location to the accuracy desired remains elusive, primarily because the ray paths have not been determined sufficiently accurately but also because the pattern of rays that arise for even simple refractive-index profiles is intricate, thus making the task of inverting an image difficult; see for example Figure 4. An explicit asymptotic-solution determination of the ray path for quadratic index profiles on a spherical Earth recently obtained by Nener *et al.* [1] greatly simplifies the problem. We will briefly describe

this work and then go on to discuss its use for image inversion for general (radially varying) refractive-index profiles.

Refractive-index variations arise because the speed of ray propagation is (weakly) dependent on the temperature, pressure and humidity of the atmosphere through which the ray is propagating[1]; see [2] for the optical case. Significant changes in such climatic conditions occur especially close (and parallel) to the Earth's surface, with temperature variations being dominant in the optical ray propagation context. In the atmospheric-boundary-layer context of interest here the refractive index model

$$n = 1 + \upsilon n', \quad \text{with } n' = \gamma \frac{P}{T}, \quad \text{where } \upsilon = 10^{-6} \text{ and } \gamma \approx 78,$$

is accurate; see [3, p. 354]; here P is the pressure in mbars and T is the absolute temperature in Kelvin. The refractive-index variations are relatively small (of order υ), so that the deviation of a ray from a straight-line path is small; however, such small deviations are sufficient to lead to deflections of the order of meters over the propagation distances (20–30 km) of interest, and give rise to optical distortions and in some situations, inversions and mirages. Also over the distances of interest the curvature of the Earth cannot be ignored; indeed, a determination of the viewing horizon is often high on the list of priorities. Temporal variations in refractive index due to turbulence result in variations in the image position (shimmering or dancing) and intensity (twinkling or scintillation). Such temporal issues will not be addressed, but asymptotic techniques along the lines described here are likely to lead to practically useful descriptions for such phenomena.

1.1. Previous work

Snell's Law (when modified for spherical geometry) says

$$Rn(R)\cos\gamma(R) = c \tag{1}$$

along a ray, where R is the radial distance within the atmosphere from the Earth's centre, $n(R)$ is the refractive index, $\gamma(R)$ is the angle of the ray with respect to the local horizontal, and c is a constant for the ray. This equation determines the deviation of the propagating ray locally, so that in theory the complete path can be determined by patching together local solutions numerically (see Lehn [4]) or by integrating Snell's Law. An exact solution is, however, unavailable except in the constant-refractive-index case. The practical difficulty is that *very* accurate evaluations are required in order to quantitatively interpret visual observations. Earth-curvature effects introduce a further source of numerical inaccuracy. In short, numerical ray tracing and integration calculations run into accuracy problems of both a truncation and round-off type. Even if such calculations are performed to the required accuracy, they are unlikely to lead to a practical understanding of the effect of atmospheric variations on the quality of the image. Such difficulties are compounded when one attempts to solve the inverse problem using forward solutions to home-in on the required refractive-index profile.

Early investigations of atmospheric propagation were made by Nölke [5] in 1917 using a flat-Earth model, valid for short ranges. Kerr [6, Section 1.5, pp. 15–22] used the concept of Modified Index of Refraction N (originally due to Schelling *et al.* in 1933 [7]) to take into account the Earth-curvature effect, reducing the problem again to rectangular coordinates but with an extended range of applicability. Since that time a number of approaches to the solution of the forward problem have been taken; see [4, 8–18]. Of particular note is the extension by Kropla and Lehn [19] of the parabolic-ray-curvature approach of Lehn [4], applicable

[1]And also the wavelength of the propagating ray.

to spherical layers containing constant refractive-index gradients. These approaches have the difficulty that the approximations are local and require accurate numerical patching to realize an acceptable output for general profiles. Recently the authors have obtained accurate explicit asymptotic solutions for the complete ray path for quadratic refractive index profiles; see [1]. The extension to quadratic refractive-index profiles is important because the received images in this case are uniformly magnified, thus greatly facilitating the construction of and inversion of an image; quadratics are optimal.[2] These results will be described here briefly before proceeding on to the main body of this work.

In Section 2 we describe the scaling and approximation ideas that lead to a simplified description of the path of rays propagating through a radially varying refractive-index medium over the Earth, and use the results to determine an explicit path description for rays propagating through a medium described by quadratics and then patched quadratics. In Section 3 we show how these results can be used to invert an image generated by such rays.

Rapid refractive-index changes sometimes occur within boundary layers a few meters thick close to the surface of the Earth, and mirages can result. In Section 4 we use asymptotic-matching principles to examine such situations.

2. Ray paths in radial refractive-index cases

Optics is, of course, one of the classic topics of physics and perhaps the earliest, and arguably the most significant, application area for asymptotic techniques. The wave length of light is of the order of 10^{-7} m; very much smaller than propagation distances of normal interest. Short-wave asymptotic (WKBJ) approximations utilize this large difference in scales to obtain an extremely accurate,[3] and very much simplified, description of the wave field. Except very close to caustics and other regions of focusing and shadow boundaries, a ray-path (or Geometric Optics) description suffices with the rays coinciding with the characteristics of the eikonal equation

$$(\nabla\psi)^2 = n^2(\mathbf{r}). \tag{2}$$

In the particular case of interest here, in which the refractive index varies only with distance R from the centre of the Earth, the characteristic equations can be integrated to give an *implicit* description for the ray path $R(\theta)$, where θ is the angular displacement away from the launch position; see Figure 1. If the ray is projected from $(R,\theta) = (R_0, 0)$ at a launch angle whose tangent is γ_0 (see Figure 1) then

$$\int_{R_0}^{R} \frac{q_0 \, \mathrm{d}R'}{R'^2\sqrt{(n^2(R') - q_0^2/R'^2)}} = \pm\theta, \quad \text{with } q_0 = R_0(1+\upsilon n')\cos\gamma_0, \tag{3}$$

where the sign needs to be chosen so that at $\theta = 0$, the angular displacement of the ray $\gamma = \gamma_0$. This well-known result can also be obtained by directly integrating Snell's Law (1).

An explicit evaluation of the integral in (3) is not possible, except in the constant refractive-index ($n = 1$) case, which yields the expected straight-line solution $R^1(\theta)$ given by

$$q_0/R^1 = \cos(\gamma_0 \pm \theta). \tag{4}$$

Whilst exact, the above ray-path description (3) is not suitable for evaluation because of the large and small variables and parameters sprinkled throughout the expression.

[2]Higher-order profiles give rise to distorted images.
[3]Relative error of order 10^{-7}.

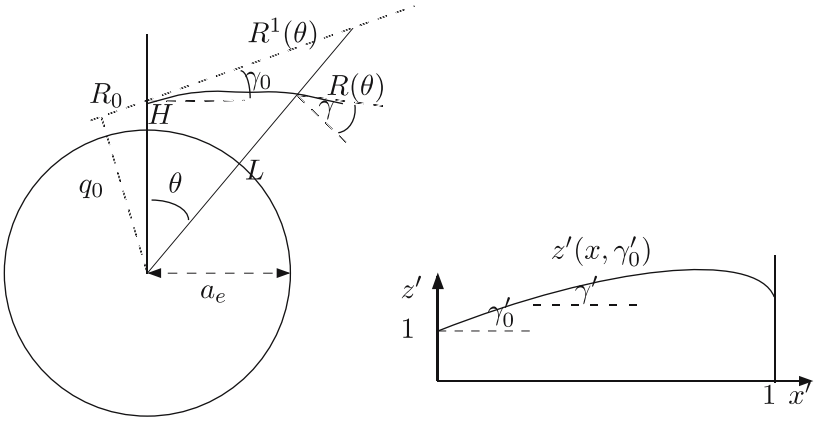

Figure 1. Ray propagation around the Earth: *Left:* Unscaled geometry. The ray $R(\theta)$ is launched from $(R,\theta) = (R_0, 0)$ at a height H above the Earth to a target at distance L around the Earth. The tangent of the initial launch angle is γ_0. $R^1(\theta)$ is the straight-line ray path in the constant refractivity case. *Right:* The ray path in the scaled domain.

2.1. Scaling

Typically we are interested in waves propagating over distances $L \approx 10\,\text{km}$, at heights $H = R_0 - a_e \approx 10\,\text{m}$, over the Earth, a sphere of radius $a_e \approx 6 \times 10^3\,\text{km}$, within an atmosphere with refractive-index variations of the order 10^{-6}. With this in mind, we introduce scaled coordinates (x', z'), with x' measuring distance from the source location measured around the surface of the Earth and scaled so that $x' = 1$ is the location of the target, and z' the height above the surface, scaled so that $(0, 1)$ is the location of the source; see Figure 1. To do this we write

$$R = a_e(1 + (hl)z'), \quad \theta = lx', \quad \gamma_0 = h\gamma_0', \quad n = 1 + \upsilon n'(z'), \tag{5}$$

$$\text{where} \quad \upsilon = 10^{-6}, \quad \text{and where } l = \frac{L}{a_e} \text{ and } h = \frac{H}{L} \tag{6}$$

are both of order 10^{-3}. We also scale the refractive index variations to reflect the expected range by writing the refractive index in terms of the *refractivity* n';

$$n = 1 + \upsilon n', \quad \text{with } \upsilon = 10^{-6}. \tag{7}$$

After changing to scaled variables and expanding out in terms of the small parameters (h, l, υ), the ray-path equation (3) reduces to

$$x' = \int_1^{z'} \frac{1}{\gamma'(n'(u'))}\,\mathrm{d}u' + O(\upsilon, hl), \text{ where} \tag{8}$$

$$\gamma' = \pm\sqrt{[2\eta(n'(z') - n'(1)) + 2\kappa(z' - 1) + (\gamma_0')^2]} \tag{9}$$

can be interpreted as the tangent of the angle the ray path makes with the horizontal at any location (x', z'); see Figure 1. Here

$$\eta = \frac{\upsilon L^2}{H^2}, \quad \kappa = \frac{L^2}{a_e H}, \tag{10}$$

are the dimensionless groups of the problem: η is a refractivity variation parameter and κ a curvature parameter; $\kappa = 0$ corresponds to a flat-Earth approximation.

Note that a prescribed ray, identified by its initial projection angle γ_0', cannot propagate into a region in which the argument of the square root defining γ' is negative; in fact, the ray will reach a turning point on the boundary $z' = z_t'$ of this region, so that

$$\gamma'(z_t', \gamma_0') = 0 \tag{11}$$

determines the height z_t' at which such turning points can occur; a useful result not requiring a complete path determination. The determination of the corresponding horizontal location x_t' does, however, require a path description.

The above result for the ray path may appear to be a purely superficial re-arrangement of the earlier description; however, from a numerical point of view the improvement is substantial. Both parameters η and κ in the above integral are of unit order and the integral is to be evaluated over a distance of unit order, so that an accurate numerical evaluation is possible using standard packages. If in addition the order υ, hl terms are neglected (with relative error of order 10^{-6}) the integral in the path description can be evaluated *exactly* for linear and quadratic refractive index profiles.

For future purposes it should also be noted that the path description depends on the refractive index *difference* $n'(z) - n'(1)$, so that a uniform shift in the refractive-index profile will not affect ray-paths. One implication is that such shifts cannot be detected by a simple ray path observation so that the inverse problem is ill-posed; an independent measurement of the datum $n'(1)$ is necessary for a complete profile determination.

For convenience we will now drop all primes on scaled quantities.

2.2. Analytic solutions for quadratic index profiles

A great advantage of the approximate ray-path description (8) is that exact solutions are available for simple index profiles of practical importance, and the result for quadratic index profiles is especially significant. Explicitly, if the profile (after scaling) is given by

$$n(z) - n(1) = a_2(z-1)^2 + a_1(z-1), \tag{12}$$

then the integral in (8) can be evaluated and the result obtained inverted to give the explicit path description

$$z(x, \gamma_0) - 1 = \left[\frac{\sin(\sqrt{-2\eta a_2}x)}{\sqrt{-2\eta a_2}}\right]\gamma_0 + \zeta(\cos\sqrt{-2\eta a_2}x - 1), \quad \text{if } a_2 < 0, \tag{13}$$

and

$$z(x, \gamma_0) - 1 = \left[\frac{\sinh(\sqrt{2\eta a_2}x)}{\sqrt{2\eta a_2}}\right]\gamma_0 + \zeta(\cosh\sqrt{2\eta a_2}x - 1), \quad \text{if } a_2 > 0, \tag{14}$$

where

$$\zeta = \frac{\eta a_1 + \kappa}{2\eta a_2}. \tag{15}$$

In the linear limit, $a_2 = 0$, the familiar parabolic profile

$$z - 1 = \frac{1}{2}[(\kappa + \eta a_1)x^2 + 2\gamma_0 x],$$

or

$$x(\gamma_0) = \frac{1}{\eta a_1 + \kappa}\left(\sqrt{\gamma_0^2 + 2(\eta a_1 + \kappa)(z-1)} - \gamma_0\right), \tag{16}$$

is recovered.

Note that the path description does not contain the constant $n(1)$; as indicated earlier a uniform shift in refractive index profile does not effect the ray path. The two cases $a_2 > 0$ and $a_2 < 0$ are very different; see Figures 2 and 3.

2.2.1. *The concave profile case ($a_2 > 0$)*
In this case the refractive index increases away from an effective minimum located at $z = 1 - a_1/(2a_2)$; see (12). Rays which deflect towards higher-index regions spread out and away from this location; see Figure 2.

2.2.2. *The convex profile case ($a_2 < 0$)*
In this case the refractive index decreases away from an effective maximum located at $z = 1 - a_1/(2a_2)$; rays bend back towards this location, leading to oscillatory behaviour with

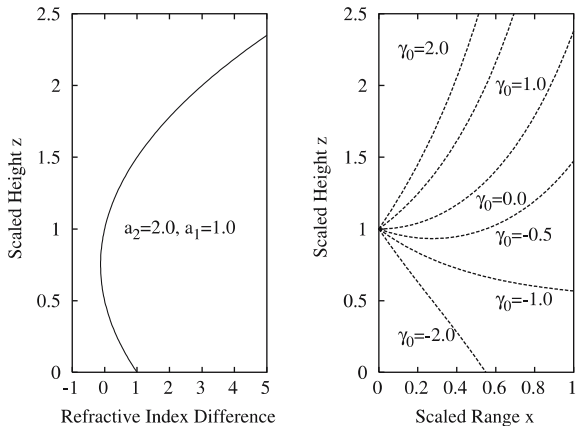

Figure 2. Quadratic Index Profile Rays: Concave profile ($a_2 > 0$) case. *Left:* The index profile ($a_1 = 1{\cdot}0,\ a_2 = 2{\cdot}0$). *Right:* Rays are launched from height $z = 1{\cdot}0$ with a range of initial angles $\gamma_0 = -2 \ldots 2$. ($\kappa = 1, \eta = 1$).

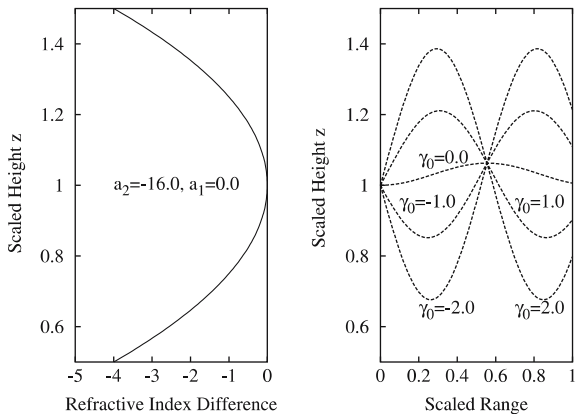

Figure 3. Quadratic Index Profile Rays: Convex profile ($a_2 < 0$) case. *Left:* The index profile ($a_1 = 0{\cdot}0, a_2 = -16{\cdot}0$). *Right:* Rays are launched from the height $z = 1{\cdot}0$ with a range of initial angles $\gamma_0 = -1 \ldots 1$ ($\kappa = 1, \eta = 1$).

period $\sqrt{-2\eta a_2}/2\pi$; see Figure 3. In this case rays intersect; in fact, all rays intersect at common intersection points. Note that, if an observer and object are located on opposite sides of an intersection point, then the observer will see an inverted image of the object; mirages are possible. Also note that, because the rays are ducted, they can propagate well beyond the normal horizon on a spherical Earth. Also, such trapped rays cannot escape the duct, so that regions of the object plane are obscured from an observer. An object located at an intersection point, for example, would be essentially invisible to an observer.

The behaviour described above was in general terms recognized going back at least to Snell, and it has recently been quantified and the results verified experimentally. However, because accurate analytic solutions for complete ray paths have not been available until the above work, numerical evaluations were needed for even linear profiles; see [4]. The truncation and numerical errors introduced made the inverse problem difficult. Given the long history, it is really surprising that the simple exact result described above had not been obtained much earlier. *Aside:* It should be pointed out that scattering and absorption effects ignored in the present work will reduce the amplitude of the propagating ray and thus the extent of ducting. Also temporal and 3D effects will affect the extent of focusing. Of course, the above theoretical results provide required information for assessing such effects.

Of particular interest to us for later work is the parametric dependence of the image height at the target end, $x=1$, as a function of the launch angle γ_0 and the profile parameters. The Equations (13–15) give

$$z(1,\gamma_0)-1=\begin{cases}\zeta(\cos\sqrt{-2\eta a_2}-1)+\left[\dfrac{\sin(\sqrt{-2\eta a_2})}{\sqrt{-2\eta a_2}}\right]\gamma_0 & \text{for } a_2<0\\[2ex] \zeta(\cosh\sqrt{2\eta a_2}-1)+\left[\dfrac{\sinh(\sqrt{2\eta a_2})}{\sqrt{2\eta a_2}}\right]\gamma_0 & \text{for } a_2>0\end{cases}, \tag{17}$$

with

$$\zeta=\frac{\eta a_1+\kappa}{2\eta a_2}.$$

2.3. General profiles: patched quadratics

Exact ray-path solutions can be obtained for up to quartic refractive-index profiles using (8), but for practical purposes such profile representations and results are not likely to be of use. A *much* to be preferred procedure is to break up the refractive-index domain into a small number of sensible horizontal layers and to describe the profile in each of the layers using quadratics. In fact, patched quadratics represent the natural or *optimal* setting for the problem because:

- By using the above results *exact* ray-path solutions can be obtained for *any* patched quadratic profile[4]
- Patched quadratics are likely to be adequate to represent almost any index profile of practical interest.
- *The image generated by rays passing through a single quadratic layer is undistorted*; higher-order profiles produce distorted images. This result, which will be established in the next section, *greatly* facilitates both the generation of ray paths and image inversion.

For practical purposes no more than three or four layers should be necessary to represent the index profile; we will number these layers from the Earth up. Explicitly we use

$$n^{(i)}(z)=a_2^{(i)}(z-1)^2+a_1^{(i)}(z-1)+c^{(i)},\quad \text{for } z_1>z>z_{i-1},\ i=1,2,\cdots \tag{18}$$

[4]The procedure becomes impractical for large numbers of layers.

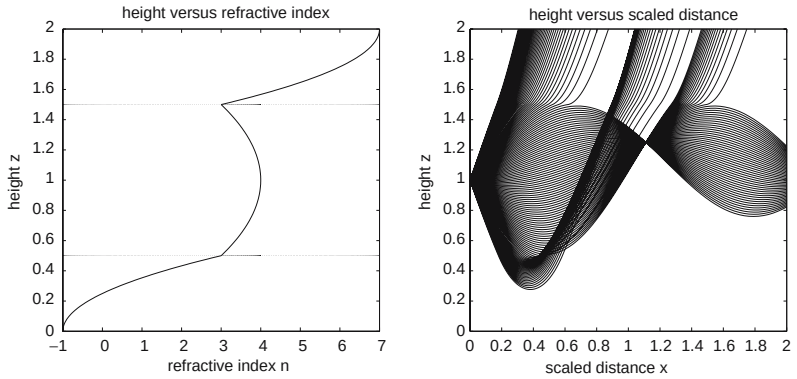

Figure 4. Propagation through three quadratic index layers: *Left:* The refractive index profile. *Right:* Rays projected into the domain.

Normally the quadratic representations should be chosen so that the profile is continuous across the layers; the constants $c^{(i)}$ can be chosen to achieve this end.[5] With this choice the ray path through any finite number of quadratic zones can be exactly determined by simply matching the location and slope of rays described by (13, 14) across the quadratic zones, and thus complete images can be generated for any patched quadratic profile. A simple program that does just this has been written and the results are displayed in Figure 4 for a case involving three layers. The computation is effectively instantaneous on a desktop computer, as one would expect.[6] In the case shown, rays with a variety of launch angles are projected into layer 2, a convex index-profile layer. For moderate launch angles the rays are trapped within the layer. For sufficiently large launch angles rays escape from layer 2 into layer 3, never to return. For sufficiently small launch angles rays penetrate into layer 1 and are then deflected back into layer 2 and finally into layer 3. It is interesting to note that the pattern of rays generated by such a simple index profile is quite complex.

3. Image reconstruction

The aim of the present work is to unscramble the image of an object generated by rays propagating through a radially varying refractive-index profile. The task could be considered to be complete if one could use the results so far obtained to determine the image of the same object that would be generated under uniform refractive-index conditions. In order to construct this true image, we need to determine the refractive-index profile. We have already seen that a uniform shift in this profile[7] cannot be detected; however, such a shift does not affect the image, and so there is no need to make such a determination in context. The aim is thus to determine the refractive-index-profile parameters $(a_1^{(i)}, a_2^{(i)})$, $i = 1, 2, \ldots$, and the layer thicknesses, in terms of observable image characteristics. We will commence by considering the single-layer case.

The observation instrument used to view an object normally consists of a lens or mirror system to produce a real image, and an array of photodetectors (perhaps the retina or a photographic plate) in the image plane to detect the image. For purposes of exposition the object being viewed is a lighthouse with equally spaced markings up its side and located at a

[5]Recall that a shift in the refractive-index profile does not effect ray paths.
[6]Schemes based on local path descriptions are of course computationally intensive.
[7]That is a change in $n(1)$.

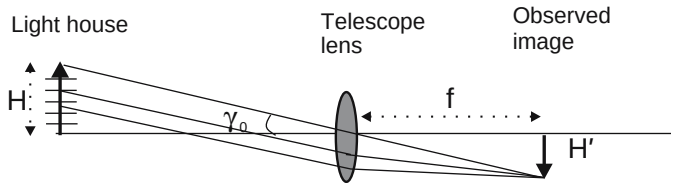

Figure 5. The ideal observation system. An image is formed on the focal plane of the lens.

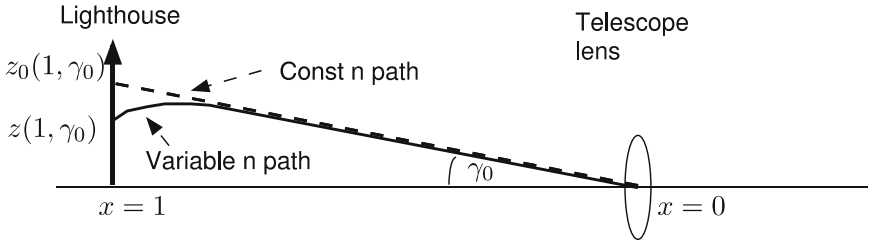

Figure 6. The ideal ray path (constant refractive index) and the actual ray path for a radially varying refractive-index profile.

distance sufficiently far away from the observation system that the image occurs in the focal plane of the optical system; see Figure 5. Our interest is in atmospheric refraction effects rather than in the flaws of the observation system due to focusing problems, so that we will assume the system is ideal in the sense that all rays from a particular marking on the lighthouse converge to a single point on the focal plane after passing through the 2D lens.[8] With this system the lens simply converts the angle γ_0 subtended by the ray passing through the centre of the lens into a corresponding image height H' in the focal plane given by $\tan\gamma_0 = \frac{H'}{f}$, where f is the focal length of the lens; see Figure 5.[9]

If we equate the incoming or entry angle at the lens to the source launch angle as defined in our earlier work, then all our previous results for ray paths carry across immediately to this situation with the lens being located at $(0, 1)$, and with $z(1, \gamma_0)$ now representing the scaled height of the viewed object above the Earth.

Now under uniform refractive-index conditions the ray entering the lens at angle γ_0 arrives from the location in the object plane $z = z_0(1, \gamma_0)$ given by

$$z_0(1, \gamma_0) = 1 + \kappa/2 + \gamma_0; \tag{19}$$

see (16) with $a_1 = 0$, and Figure 6. The axis of the lens given by $\gamma_0 = 0$ provides an appropriate datum for vertical location in the object plane so that there is an apparent vertical displacement in the object plane given by $z_0(1, 0) - 1 = \kappa/2$, due to the Earth's curvature.[10] Also note that the resulting scaled magnification is given by $\frac{\mathrm{d}z_0(1,\gamma_0)}{\mathrm{d}\gamma_0} = 1$, so that equally spaced markings on the lighthouse will be seen as equally spaced markings in the image plane; see Figure 7. The received image will be uniformly magnified.

[8]We also ignore 3D effects. Note also that the range here is large.
[9]Thus $H' = (f/L)H$ under constant refractive index, flat Earth ($\kappa = 0$) conditions, where L is the distance of the lighthouse from the lens; a uniformly magnified image is received.
[10]Recall that $z = 1$ is the location of the lens.

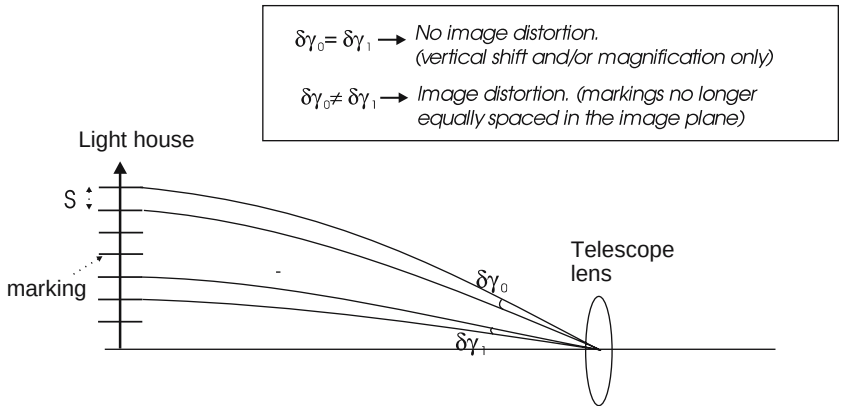

Figure 7. Optical distortion: the figure depicts rays propagating from equally spaced markings on a lighthouse to the observation lens.

In our variable refractive-index-medium case the ray entering the lens at angle γ_0 arrives from the location in the object plane given by $z(1,\gamma_0)$, so that there is an additional apparent vertical displacement[11] in the object plane due to refractivity effects given by $z(1,\gamma_0) - z_0(1,0)$, where we have chosen $\gamma_0 = 0$ as a datum. By writing this in the form

$$z(1,\gamma_0) - z_0(1,0) = \mathcal{D}(n) + \mathcal{M}(n,\gamma_0)\gamma_0,$$

we can identify the offset or apparent displacement $\mathcal{D}$ and the local magnification $\mathcal{M}$ due to refraction. In general, we would expect the magnification $\mathcal{M}$ to vary with the entry angle γ_0, resulting in a non-uniformly magnified or distorted image, but for the quadratic case using (17) we get

$$\mathcal{M}(a_2) = \frac{\sin\left(\sqrt{-2\eta a_2}\right)}{\sqrt{-2\eta a_2}}, \quad \mathcal{D}(a_1,a_2) = \frac{\eta a_1 + \kappa}{2\eta a_2}\left[\cos\sqrt{-2\eta a_2} - 1\right] - \frac{\kappa}{2}$$

in the $a_2 < 0$ case, and

$$\mathcal{M}(a_2) = \frac{\sinh\left(\sqrt{2\eta a_2}\right)}{\sqrt{2\eta a_2}}, \quad \mathcal{D}(a_1,a_2) = \frac{\eta a_1 + \kappa}{2\eta a_2}\left[\cosh\sqrt{2\eta a_2} - 1\right] - \frac{\kappa}{2}$$

in the $a_2 > 0$ case. Note that in the limit as $a_2 \to 0$, $\mathcal{D} \to \frac{\eta a_1}{2}$ and $\mathcal{M} \to 1$.

Thus *the image generated by rays propagating through a quadratic index profile is uniformly magnified*. For higher-order profiles distortion occurs. Now we all know that images are true in a constant refractive-index flat-Earth situation,[12] and many would be aware of the somewhat surprising result that images are also true in the linear refractive-index profile flat-Earth situation, where rays are parabolic. Remarkably, however, this is also the case for quadratic refractive-index situations over a spherical Earth! Observing the converging and diverging behaviour of propagating rays (see Figures 2 and 3) this would seem to be unlikely.

The magnification and displacement results are plotted in Figure 8. Note that the magnification is dependent only on a_2, and is unity if $a_2 = 0$, that is, for linear refractivity profiles. For fixed a_2 the displacement varies linearly with a_1. Note also that the displacement is

[11] Added on to the apparent displacement due to the Earth's curvature.
[12] Where the rays are straight lines.

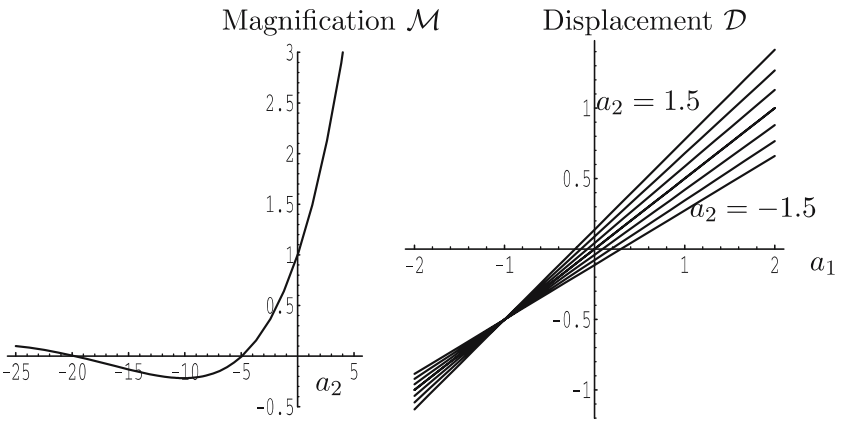

Figure 8. Left: The variation of image magnification $\mathcal{M}$ with a_2. *Right:* The variation of displacement $\mathcal{D}$ with a_1 for $-1{\cdot}5 < a_2 < 1{\cdot}5$ ($\kappa = 1, \eta = 1$).

equal to $-\kappa/2$ when $a_1 = -\kappa/\eta$ for all values of a_2. This situation is the one in which Earth-curvature effects and refractivity effects just balance. Using these results, it is a trivial matter to determine the refractivity coefficients a_1, a_2 for any quadratic profile using observations of the magnification and displacement. One simply first uses the observed magnification to determine a_2. The appropriate displacement curve can then be used to determine a_1 from offset observations. It should be noted that in the $a_2 < 0$ oscillatory-path case there are several choices for a_2 that give identical magnification, so some care is required. Of course, having determined (a_1, a_2) it is a trivial matter to determine a true image.

At least for quadratic profiles the inverse problem is solved and ray-path computations are not even required to invert an image.

3.1. Inversion of general profiles

For refractive-index profiles more complex than a simple quadratic, the received image will be distorted. It should be noted, however, that rays received from the object plane that remain within one of the quadratic layers will generate an undistorted image whose displacement and magnification can be used to determine the index coefficients $\left(a_1^{(i)}, a_2^{(i)}\right)$ for that layer. We will refer to rays that separate out significant regions in the propagation region as *critical rays*, and will also refer to the associated entry angles as being critical. Rays with turning points located on the Earth's surface, or on other significant profile-change interfaces, are thus critical. Observations of *critical rays* can be used to determine the locations of edges of the layers. No attempt will be made here to detail the inversion process in the general patched quadratic case but, in principle, the procedure is straightforward. In practice the location of the observation system can strongly affect the outcome.

We will illustrate the procedure by referring back to the example shown in Figure 4. Rays propagating entirely within the convex refractive-index layer ($0{\cdot}5 < z < 1{\cdot}5$) produce a constant magnification image in the image plane; observations can be used to determine $\left(a_1^{(2)}, a_2^{(2)}\right)$. The critical rays bounding this propagation zone have turning points located on the edges of layer 2, so that observations of the critical angles, when used in association with the turning-point result (11), will determine the boundaries of layer 2 (in this case $z = 0{\cdot}5$ and $z = 1{\cdot}5$). Rays entering the lens at angles outside the above range arrive from regions of the object plane that are remote from those that are trapped within the convex zone, so that the image will contain discontinuities corresponding to the above critical angles. Furthermore,

the received images associated with these rays will be distorted because they pass through more than one layer. Whilst it is a straightforward matter in theory to trace the path of a ray through two or more layers, and thus determine the resulting local image magnification, such a procedure is unlikely to be useful in practice for image inversion. To determine the refractive-index parameters corresponding to layers 1 and 3 one would need to receive useful (relatively undistorted) magnification information from the object plane and this is best achieved by relocating the observation system.

In general, singularities (or catastrophies) in the propagation domain correspond to refractive-index-profile transitions or are associated with domain boundaries. A classification of the singularities of the map (13, 14) from $(n(z), \gamma_0)$ to $z(1, \gamma_0)$, with $n(z)$ piecewise quadratic, would be valuable. The parameter γ_0 is a bifurcation parameter for the problem. This study is under way.

4. Boundary-layer effects: the inferior mirage

Very high temperatures close to a road surface cause refractive-index decreases that can result in mirages. Typically, the refractive-index profile decreases exponentially within a boundary layer of thickness 0·5–2 m. A suitable model for refractive-index variations inside the boundary layer, and for moderate distances above the road surface is given by

$$n(z) = n(1) + a_1(z-1) - \delta n \ \mathrm{e}^{-\frac{z}{\epsilon}}, \tag{20}$$

where $n(1) - a_1$ is the refractive index at the road surface if local surface effects are ignored, and δn is the change in refractivity across the boundary layer of thickness ϵ, which we assume to be small.[13] We will assume $\delta n > 0$; in this case rays entering the boundary layer will be deflected away from the surface of the Earth, so that mirages are possible. The ray-path integral (8) cannot be exactly evaluated for this linear/exponential profile; however, in the constant/exponential case the integral can be exactly determined and, by utilizing the smallness of ϵ, we can use asymptotic matching to facilitate the analysis of the problem.

As with the earlier work an accurate determination of ray paths is required to invert an image. We already have an accurate description of the path of rays that do not enter the boundary layer, so that a determination of the path of rays that enter the boundary layer and then later emerge is required; see Figure 9. These rays are effectively reflected by the boundary layer. Such rays have a turning point within the boundary layer which we will denote by (x_t, z_t). With $n(z)$ as above, see (20), the angular displacement[14] away from the horizontal of a ray at any location z when launched at angle γ_0 is given by

$$\gamma(z) = -\sqrt{\gamma_0^2 + 2(z-1)(\eta a_1 + \kappa) - 2\eta \ \delta n \ \mathrm{e}^{-z/\epsilon}}, \quad \text{for } x < x_t, \tag{21}$$

see (9, 20), so that the rays of interest are those with launch angles $\gamma_0(z_t)$, obtained by solving

$$\gamma_0^2 + 2(z_t - 1)(\eta a_1 + \kappa) - 2\eta \ \delta n \mathrm{e}^{-z_t/\epsilon} = 0 \tag{22}$$

for $\gamma_0(z_t)$, where z_t spans the boundary layer. The range of associated launch angles is of unit order because the change of refractivity is of unit order across the boundary layer. We will denote the launch angle associated with the turning point (x_t, z_t) by γ_{0t}, so $\gamma_{0t} \equiv \gamma_0(z_t)$. The

[13] So that the thickness of the boundary layer is much smaller than the viewing height H.
[14] really the tangent of the angular displacement, but to first order these are equal.

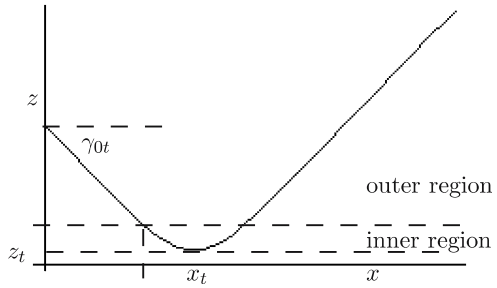

Figure 9. A ray entering the boundary layer, turning at (x_t, z_t), and emerging.

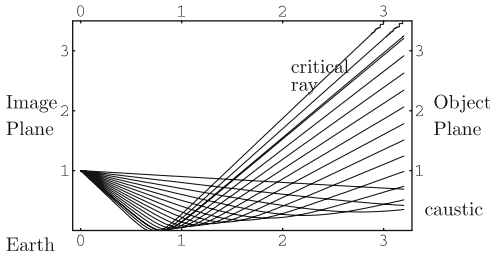

Figure 10. Rays propagating through an exponential boundary layer from an object plane at $x = 4$ to a lens at $(0, 1)$. $(\eta = -1, \epsilon = 0{\cdot}1,\ \kappa = 0, a_1 = 0$ with $\gamma = -1{\cdot}2, -1, -0{\cdot}8, -0{\cdot}6, -0{\cdot}4, -0{\cdot}2, -0{\cdot}1)$.

ray that has a turning point located on the surface of the Earth is a *critical ray*. The launch angle corresponding to this critical ray is given by

$$\gamma_{0\text{crit}} = -\sqrt{2(\eta a_1 + \kappa) + 2\eta\ \delta n}. \tag{23}$$

Rays with initial launch angles γ_0 less than the *critical angle* will strike the Earth and will be absorbed.

4.1. The outer solution description

To first order in ϵ the path description of the rays of interest in the outer region[15] is given by ignoring the exponentially small term in the expression for $n(z)$, so that we recover the linear-profile result

$$x(\gamma_{0t}) = \frac{1}{\eta a_1 + \kappa}\left(\sqrt{\gamma_{0t}^2 + 2(\eta a_1 + \kappa)(z-1)} - \gamma_{0t}\right) \tag{24}$$

for the rays; see (16). If such rays were not deflected within the boundary layer, they would hit the boundary $z = 0$ at the location $x_{\text{in}}(z_t)$ given by

$$x_{\text{in}} = \frac{1}{\eta a_1 + \kappa}\left(\sqrt{\gamma_{0t}^2 - 2(\eta a_1 + \kappa)} - \gamma_{0t}\right), \tag{25}$$

and at an angle $\gamma_{\text{in}}(z_t)$ given by

$$\gamma_{\text{in}} = -\sqrt{\gamma_{0t}^2 - 2(\eta a_1 + \kappa)}, \tag{26}$$

see (21), so that to first order in ϵ just outside the boundary layer, the ray paths of interest are given by

$$x - x_{\text{in}} = \frac{1}{\gamma_{\text{in}}} z + O(\epsilon^2), \tag{27}$$

with $(x_{\text{in}}(z_t), \gamma_{\text{in}}(z_t))$ as defined above identifying specific rays. This result will be used later for matching. This completes the description of the reflected rays in the outer region. Higher-order terms can be obtained but are not required here.

[15]That is the region outside the boundary layer.

4.2. The ray description within the boundary layer

In the boundary layer or inner region we wish to determine the ray-path description that matches onto the above outer ray description for each of the reflected rays. The ray path through the turning point (x_t, z_t) is given by

$$x - x_t = \int_z^{z_t} 1/\gamma(u)\mathrm{d}u \quad \text{for } x < x_t,$$

see (8), after adjusting the integration constant so that at (x_t, z_t) lies on the path. The actual value for x_t will be determined later. To obtain an inner approximation we re-scale the variables ($u = \epsilon v,\ z = \epsilon\zeta, z_t = \epsilon\zeta_t$) to give

$$x - x_t = \epsilon \int_\zeta^{\zeta_t} \frac{\mathrm{d}v}{\sqrt{(\gamma_{\mathrm{in}})^2 - 2\eta\delta n \mathrm{e}^{-v} + \epsilon 2(\eta a_1 + \kappa)v}},$$

see (21), where for convenience we have replaced γ_{0t} by γ_{in}, using (26). To first order in ϵ the linear term in v in the integrand can be neglected, giving

$$x - x_t = \frac{\epsilon}{\gamma_{\mathrm{in}}} \int_\zeta^{\zeta_t} \frac{\mathrm{d}v}{\sqrt{1 - \xi \mathrm{e}^{-v}}} + O(\epsilon^2), \quad \text{where } \xi = \frac{2\eta\ (\delta n)}{(\gamma_{\mathrm{in}})^2}, \tag{28}$$

and the integral evaluated to give

$$x - x_t = -\frac{2\epsilon}{\gamma_{\mathrm{in}}} \left(\operatorname{arctanh}\sqrt{1 - \xi \mathrm{e}^{-\zeta}} - \operatorname{arctanh}\sqrt{1 - \xi \mathrm{e}^{-\zeta_t}} \right), \tag{29}$$

to order ϵ^2.
Note that $\xi = 1$ corresponds to the *critical ray*.

4.3. Matching

For large ζ

$$\operatorname{arctanh}\sqrt{1 - \xi \mathrm{e}^{-\zeta}} \sim \frac{\zeta}{2} + \log \frac{2}{\sqrt{\xi}}, \tag{30}$$

so that on the outer edge of the boundary layer the inner solution for the ray path (29) is given by

$$x - x_t = \frac{z}{\gamma_{\mathrm{in}}} + \frac{2\epsilon}{\gamma_{\mathrm{in}}} \left(-\frac{\log 2}{\sqrt{\xi}} + \operatorname{arctanh}\left(\sqrt{1 - \xi \mathrm{e}^{-\zeta_t}} \right) \right) + O(\epsilon^2), \tag{31}$$

after converting back to the unstretched variable z. The choice of x_t given by

$$x_t = x_{\mathrm{in}}(\gamma_{0t}) + \frac{2\epsilon}{\gamma_{\mathrm{in}}} \left(-\frac{\log 2}{\sqrt{\xi}} + \operatorname{arctanh}\left(\sqrt{1 - \xi \mathrm{e}^{-z_t/\epsilon}} \right) \right) + O(\epsilon^2), \tag{32}$$

ensures this description matches onto the description of the rays just outside the boundary layer (27) to order ϵ^2. Note especially that the angular displacements match. Recall that $x_{\mathrm{in}} = x_{\mathrm{in}}(z_t)$ and $\gamma_{\mathrm{in}} = \gamma_{\mathrm{in}}(z_t)$ as given by (25, 26) identify specific reflected rays. The matching is now complete to first order in ϵ. The path of the ray which turns at a height z_t above the Earth is given by (24) outside the boundary layer, and (29, 32) within the boundary layer. This solution is valid for $x < x_t$. Ray paths are symmetric about $x = x_t$ so the solutions for $x > x_t$ are mirror images of the above solutions.

Interesting features that can be extracted from the above results are; see Figure 10:

- Rays entering the boundary layer at an angle γ_{in} emerge at an angle $-\gamma_{\text{in}}$ so that they are effectively reflected. The rays are, however, displaced sideways by an amount (of order ϵ) that depends on the shallowness of the entry; see (32).
- Rays that skim the outside of the boundary layer remain within the layer longer than those that penetrate further; see (32). This means that the reflected image is inverted.
- From a quantitative viewpoint the most important ray is the *critical* ray. By observing the launch angle $\gamma_{0\text{crit}}$ associated with this ray one can determine the change in refractive index across the boundary δn; see (23).
- The reflected rays form an envelope (or caustic), the location of which can be used to determine the boundary-layer thickness ϵ; see Figure 9.
- The mirage is essentially undistorted (except for inversion), except close to the caustic.

Ray-theory predictions are incorrect close to the caustic; an infinite wave amplitude is predicted due to the convergence of the rays. The correct behaviour was first investigated by Airy and, more recently, asymptotic results were obtained by Kay and Keller [20]; see also [21, pp. 375–380]. The correct result is that the amplitude remains finite but large close to the caustic as predicted by ray theory. In the present circumstances attenuation and 3D effects (not accounted for in these simplified models) are likely to determine the structure of the caustic; however, such effects are purely local[16] and so are not of interest for the image inversion work of interest here.

We will briefly describe the image generated under mirage circumstances in the simple flat-Earth ($\kappa = 0$) constant refractivity/exponential case shown in Figure 10. For this simple case rays travel in straight lines outside the boundary layer. In the situation depicted, rays received from the object plane located at $x = 4$ pass through a lens at $x = 0, z = 1$ and are focused behind the lens. The received image consists of:

- An undistorted image of the object plane above the critical ray, generated by rays passing directly from the object plane to the lens,
- superimposed images of the object plane between the critical ray and the caustic produced by direct and reflected rays, and
- a zone below the caustic which is not imaged.

Except close to the caustic the received images are uniformly magnified with $\mathcal{M} = 1$.

5. Conclusions

The centerpiece of this work is contained in the result (8) which represents an asymptotic description of the path of a ray propagating over the Earth in a steady radially varying index profile. We have seen that the usefulness of this result arises because the description is extremely accurate and because it leads to explicit ray-path solutions for a very broad range of index profiles over a spherical Earth; see Equations (13, 14, 24, 27). This is a significant advance on earlier results in that such paths needed to be obtained by numerical integration and the resultant errors hampered image-inversion work. As an added bonus the image received through a quadratic index profile was shown to be uniformly magnified, so that simple offset and magnification observations, together with critical ray observations, can be used to determine the index profile, at least for profiles of the above type. Using these results, it is a simple matter to answer the original question posed: "where is the ship and what is its shape?", at least for steady radial profiles likely to be of practical interest.

[16]Ray theory correctly positions the caustic.

Using the above results, it should also be possible to explain better, and even quantify, a number of interesting observed phenomena due to refraction in the atmosphere, such as described for example in [22, Chapter 5]. One such phenomenon is that of looming, which describes the apparent enhanced magnification of certain objects seen on the horizon. For example in [25] there is a description and photograph of individuals walking across a sand-spit who appear to be much closer to an observer than objects known to be nearer. Given the convergence and divergence of rays seen in Figure 3 due to a simple quadratic index profile variation, this is not unexpected; however, it would appear that looming is due to the fact that the apparent position of an object is not located in the same vertical plane of the object (as implied in our earlier work), and more importantly can vary in location for objects at different distances from the observer and for different heights above the Earth; distances are thus misjudged. This occurs especially under mirage-forming conditions. A general description of this phenomenon can be found in [23, Part IV, Chapter 2]. Sodha *et al.* [24] have quantified the phenomenon for exponential profiles. Their work needs to be extended using the results obtained above. Curiosity demands that all such spectacular phenomena be quantitatively explained. An excellent description of a range of such phenomena, including looming with accompanying images, can also be found in [25].

Whilst refractive-index variations are likely to be most rapid in a direction normal to the Earth's surface, there are obvious situations in which rapid variations are likely to occur around the surface of the Earth. For example rapid changes are likely to occur where land and sea meet and, of course, marine observations are often made from the land. If the length scale of such transitions is much smaller than the horizon distance (about 20 km), then a useful description may be obtained using the above results. If this is not the case, then the approximations underlying the above work are no longer valid; accurate exact results are unlikely in such cases.

Perhaps the most promising and exciting extension to the above analysis lies in the area of scintillation. Turbulent fluctuations cause the ray paths to fluctuate, so that the image associated with a particular point object will move on the image plane, giving rise to "shimmer", "dancing" or "wandering". Fluctuations in intensity also occur. Whilst the variations are relatively small, the effect on the received image can be dramatic, and in fact the received image often can be unrecognizable. The twinkling star is, of course, the best known example. The effect would be minor if all image points moved in unison but this does not occur. It is a major task to unscramble such images. Given the results for ray paths displayed in Figures 2 and 3, one would expect variations in the average refractive index in the radial direction to strongly effect the received image; such effects have not yet been accounted for and can now be addressed using the above results. The turbulent fluctuations of interest occur over a time scale much larger than the time for a ray to pass from the object to the observation system, so that multi-scaling or averaging techniques are likely to lead to a usefully simple description for the fluctuating ray paths taking into account radial variations in the index mean. Using such an approach it should be possible to accurately filter the received image upon which a sensible attempt can be made to invert the image. This work in under way.

References

1. B.D. Nener, N.D. Fowkes and L. Borredon, Analytical models of optical refraction in the troposphere. *J. Opt. Soc. Am. A* 20 (2003) 867–875.
2. Bengt Edlen, The refractive index of air. *Metrologia* 2 (1966) 71–80.

3. R.G. Fleagle and J.A. Bussinger, *An Introduction to Atmospheric Physics* (2nd ed). New York: Academic (1980) 432 pp.
4. W.H. Lehn, A simple parabolic model for the optics of the atmospheric surface layer. *Appl. Math. Modell.* 9 (1985) 447–453.
5. Fr. Nölke, Zur Theorie der Luftspiegelungen (The theory of mirages). *Physik. Zeitschr.* 18 (1917) 134–142.
6. D.E. Kerr (Radiation Laboratory Series) (ed.), *Propagation of Radio Waves.* New York: McGraw-Hill (1951) 728 pp.
7. J.C. Schelleng, C.R. Burrows and E.B. Ferrell, Ultra-short wave propagation. *Proc. of IRE* 21 (1933) 427–463.
8. W.H. Lehn, Inversion of superior mirage data to compute temperature profiles. *J. Opt. Soc. Am.* 73 (1983) 1622–1625.
9. W.H. Lehn and H.L. Sawatzky, Image transmission under arctic mirgae conditions. *Polarforschung* 45 (1975) 120–129.
10. W.H. Lehn and J.S. Morrish, A three parameter inferior mirage model for optical sensing of surface layer temperature profiles. *IEEE Trans. Geosci. Remote Sensing* GRS-24 (1986) 940–946.
11. W.H. Lehn and M.B. El-Arini, Computer-graphoics analysis of atmospheric refraction. *Appl. Opt.* 17 (1978) 3146–3151.
12. R. White, New solutions of the refraction integral. *J. Opt. Soc. Am.* 65 (1975) 676–678.
13. A.B. Fraser, Simple solution for obtaining a temperature profile from the inferior mirage. *Appl. Opt.* 18 (1979) 1724–1731.
14. A.B. Fraser, Solutions of the refraction and extinction integrals for use in inversions and image formation. *Appl. Opt.* 16 (1977) 160–165.
15. W.H. Mach and A.B. Fraser, Inversion of optical data to obtain a micrometeorological temperature profile. *Appl. Opt.* 18 (1977) 1715–1723.
16. P.D. Sozou, Inversion of mirage data: an optimization approach. *J. Opt. Soc. Am. A* 11 (1979) 125–134.
17. C.M. Roach, W.G. Rees and C.H.F. Glover, Inversion of atmospheric refraction data. *J Opt. Soc. Am.* 8 (1991) 330–339.
18. W.G. Rees, Mirages with linear image diagrams. *J. Opt. Soc. Am. A* 7 (1990) 1351–1354.
19. Wiliam C. Kropla and Waldemar H. Lehn, Differential geometric approach to atmospheric refraction. *J. Opt. Soc. Am.* 9 (1992) 601–608.
20. I. Kay and J.B. Keller, Asymptotic evaluation of the field at a caustic. *J. Appl. Phys.* 25 (1954) 876–883.
21. Ali Hasan Nayfeh, *Perturbation Methods.* New York: John Wiley and Sons (1973) 425 pp.
22. M.G.J. Minnaert, *Light and Colour in the Outdoors.* New York: Springer-Verlag (1993) 417 pp.
23. W.J. Humphreys, *Physics of the Air.* New York: Dover (1946) 676 pp.
24. M.S. Sodha, A.K. Aggarwal and P.K. Kaw, Image formation by an optically stratified medium: optics of mirage and looming. *Brit. J. Appl. Phys.* 18 (1967) 503–511.
25. A.B. Fraser and W.H. Mach, Mirages. *Sci. Am.* 234 (1976) 102–111.